Renewable Energy 235 (2024) 121307

Contents lists available at ScienceDirect

Renewable Energy

journal homepage: www.elsevier.com/locate/renene

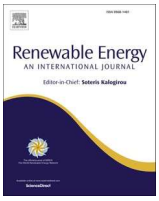

Atomically dispersed ruthenium in transition metal double layered hydroxide as a bifunctional catalyst for overall water splitting

Njemuwa Nwaji [a,*], Boka Fikadu [b], Magdalena Osial [a], Birhanu Bayissa Gicha [b], Magdalena Warczak [c], Hao Fan [d], Jaebeom Lee [e,**], Michael Giersig [a,***]

[a] Institute of Fundamental Technological Research, Polish Academy of Sciences, Pawinskiego 5B Str. 02-106, Warsaw, Poland
[b] Department of chemistry, Chungnam National University, Daejeon, 34134, South Korea
[c] Faculty of Chemical Technology and Engineering, Bydgoszcz University of Science and Technology, Seminaryjna 3 street, 85-326, Bydgoszcz, Poland
[d] State Key Laboratory for Mechanical Behavior of Materials, Shaanxi International Research Center for Soft Matter, Xi'an Jiaotong University, Xian, China
[e] Department Chemical Engineering and Applied Chemistry, Chungnam National University, Daejeon, 34134, South Korea

A B S T R A C T

Efficient and sustainable energy conversion depends on the rational design of single-atom catalysts. The control of the active sites at the atomic level is vital for electrocatalytic materials in alkaline and acidic electrolytes. Moreover, fabrication of effective catalysts with a well-defined surface structure results in an in-depth understanding of the catalytic mechanism. Herein, a single atom ruthenium dispersed in nickel-cobalt layered hydroxide (Ru-NiCo LDH) is reported. Through the precise controlling of the atomic dispersion and local coordination environment, Ru-NiCo LDH//Ru-NiCo LDH provides an ultra-low overpotential of 1.45 mV at 10 mA cm^{-2} for the overall water splitting, which surpasses that of the state-of-the-art Pt/C/RuO_2 redox couple. Density functional theory calculations show that Ru-NiCo LDH optimizes hydrogen evolution intermediate adsorption energies and promotes O-O coupling at a Ru-O active site for oxygen evolution, while Ni serves as the water dissociation site for effective water splitting. As a potential model, Ru-NiCo LDH shows enhanced water splitting performance with potential for the development of promising water-alkaline catalysts.

1. Introduction

To mitigate environmental problems caused by greenhouse gases, hydrogen is a sustainable energy alternative to traditional fossil fuel [1,2]. The most environmentally friendly and sustainable method of producing hydrogen today is electrochemical water splitting [3,4]. Water splitting generally involves two half-reactions, hydrogen evolution (HER) and oxygen evolution (OER) [4,5] with significant overpotential, and efficient catalysts are required to reduce the excess potential and accelerate the catalytic response. For hydrogen evolution reaction (HER) and oxygen evolution reaction (OER), Pt- and Ir/Ru-oxide-based catalysts are currently the benchmark materials [6–8]. However, their high cost and poor stability limit their use on a large scale. Meanwhile, the complexity of water electrolysis equipment would inevitably increase if single-function catalysts for HER or OER were used. Therefore, a potential avenue for water electrolysis has been created with dual-function catalysts with high activity for both HER and OER [9,10]. However, the anodic OER process usually suffers from sluggish kinetics and rapid deactivation of catalysts in acidic conditions when compared to the highly efficient HER process at higher proton concentrations. As a result, most reported electrochemical water splitting catalysis has been performed under alkaline conditions, which require relatively high overpotentials to simultaneously drive HER and OER reactions for practical applications [11]. Therefore, the key to efficient hydrogen production from water electrolysis is the research and development of dual-function catalysts with high activity for both HER and OER in both acidic and alkaline media.

Among various electrocatalysts, 3D transition metal based layered double hydroxides (LDH) with different metal components (such as cobalt, nickel, and iron) possess promising electrocatalytic potentials due to their unique lamellar structure and abundant active sites [12–14]. Many and varied strategies, such as the regulation of morphology, defect formation, charge transfer, etc., have been reported [15–18] with the aim to optimizing the catalytic activity in LDH for enhanced performance. Single-atom catalysts (SACs) have emerged as a promising frontier for the optimization of catalytic activity and are of

* Corresponding author.
** Corresponding author.
*** Corresponding author.
E-mail addresses: nnwaji@ippt.pan.pl (N. Nwaji), nanoleelab@cnu.ac.kr (J. Lee), mgiersig@ippt.pan.pl (M. Giersig).

https://doi.org/10.1016/j.renene.2024.121307
Received 17 May 2024; Received in revised form 14 August 2024; Accepted 4 September 2024
Available online 6 September 2024

great interest due to the suitable coordination environment, intimate interactions of single atoms with suitable supports, and exhibit quantum size effects [19–22].

The easy aggregation of individual metal atoms in SACs poses huge challenges in preparation. Interestingly, due to their 2D flat facet, ultrathin thickness, and high surface area, two-dimensional (2D) LDHs provide a favorable platform for the stabilization of SACs [20,22]. In this respect, single atom-confined 2D LDHs are an ideal model toward maximizing OER activity while reducing the number of single atoms on the support.

In this work, atomically dispersed ruthenium catalysts confined in porous NiCo LDH are prepared through a facile hydrothermal technique, followed by electrochemical deposition (Fig. 1a). Electrodeposition is much more convenient and much less expensive than other traditionally used methods, such as physical or chemical vapor deposition and co-precipitation, in the preparation of nanocatalysts. The presence of Ru single atoms and detailed local atomic structures of Ni, Fe, and Ru sites are revealed by a combined analysis of spherical aberration-corrected transmission electron microscopy and X-ray absorption fine structure (XAFS) spectroscopy. Though Ru and NiFe LDH have been considered active OER catalysts [20,22], our assemble two-electrode Ru-NiCo LDH achieves a higher current density of 10 mA cm^{-2} at a very low overpotential of 1.45 V, which is superior to the Pt/C//RuO2 redox cell for overall water splitting in alkaline media. Density functional theory (DFT) calculations and structure-activity experiment suggest that while the Co site of the Ru-NiCo LDH optimizes the favorable regulation of H adsorption energies for HER, the Ru site promotes O-O coupling due to the presence of Ru-O moieties and the Ni site act as water dissociation site (Fig. 1b). In addition, the intrinsic HER and OER activities are enhanced by the abundant number of active sites, which accelerates the water splitting kinetics. This study also provides a promising synergistic advanced electrode platform for fundamental future work on the role of isolated Ru single atoms on NiCo LDH nanosheets in the promotion of electrocatalytic water splitting.

2. Result and discussion

The single atom Ru-based catalyst was synthesized by electrodepositing Ru onto the surface of NiCo LDH nanosheet arrays grown on carbon cloth via hydrothermal technique (Fig. 1a).

To shed light on the crystalline structure of NiCo LDH and Ru-NiCo LDH, the X-ray diffraction (XRD) patterns are shown in Fig. S1. The observed crystal peaks at $2\theta = 11.3°$, 22.7°, 33.5°, 34.4°, 38.8°, 46.0°, 60.0°, and 61.3° can be unambiguously assigned to (003), (006), (101), (012), (015), (018), (110) and (113) planes of hexagonal NiCo LDH (PDF No. 38–0715). When one and 2 M concentrations of $RuCl_3$ precursor were used, the XRD pattern showed no significant change following the incorporation of Ru atoms into NiCo LDH, suggesting that Ru is atomically dispersed within NiCo LDH (Fig. S1, Top). Increasing the molar concentration to 4-fold results in emergency of new peaks at $2\theta = 43.8$ and 58.2 (Fig. S1, bottom), which can be assigned to hexagonal phase ruthenium nanoparticle [23]. This indicates that higher concentration of the Ru lead to lack of complete atomic dispersion but formation of clustered nanoparticle. A nanoflake array with an average length of 2.5 μm and an average thickness of 36 nm was observed in the scanning electron microscope image of NiCo LDH (Fig. 1c) and the corresponding Ru-deposited derivative (Fig. 1e). Elemental mapping of Ru-NiCo LDH using energy dispersive X-ray spectroscopy (EDS) reveals a uniform distribution of Ni, Co, O, and Ru (Fig. 1d). The observed lattice distance of 0.163 nm in the high-resolution transmission electron microscopic (HRTEM) images (Fig. 1f) is assigned to the (110) crystal plane of the hexagonal Ni-Co LDH [24]. The amount of loaded Ru single atoms obtained from ICP-OES was 0.3 wt% when 1 mmol L^{-1} of.

$RuCl_3$ was used in the electrodeposition. The increasing of Ru

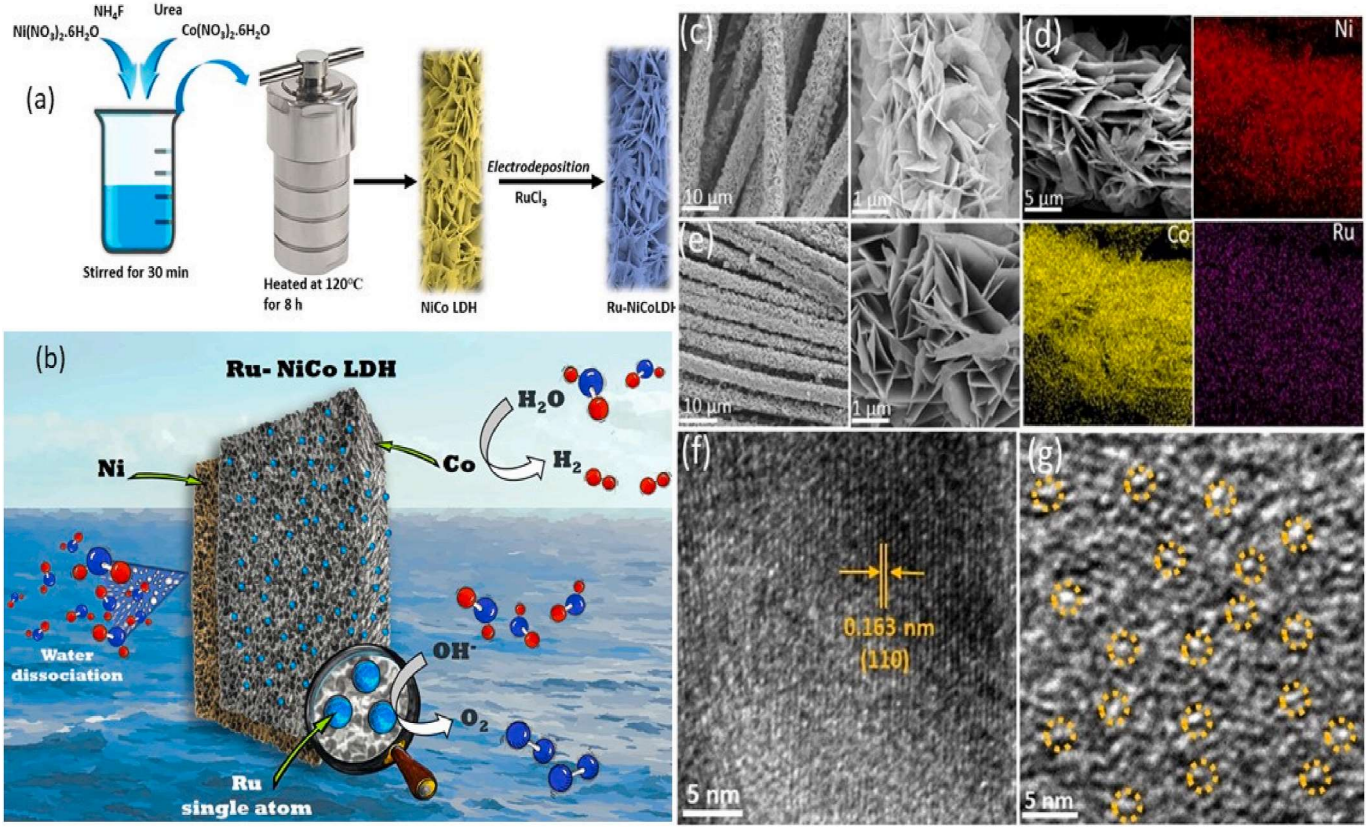

Fig. 1. Synthetic scheme and microscopic characterization (a) schematic illustration of the synthetic route for the as prepared catalyst, (b, c) SEM images of NiCo LDH and Ru-NiCo LDH, (d) EDS elemental mapping of Ru-NiCo LDH, (e) HRTEM and (f) HAADF-STEM images of Ru-NiCo LDH.

precursor concentration to 2-fold and 4-fold during the electrochemical deposition did not change the morphology of the nanoarray (Fig. S2a), and the obtained loading amount was found to be 0.52 and 1.12 wt%. The aberration corrected HAADF-STEM image (Fig. 1g) when 2 mmol of $RuCl_3$ was used clearly show isolated Ru single atom bright spots uniformly distributed on the Ru-NiCo LDH nanosheet, indicating optimal atomic dispersion of Ru single atom electrocatalyst. The HAADF-STEM image when 1 mmol $RuCl_3$ was used did not show a very clear single Ru atom while 4 mmol results in clustered particles with few single atoms (Fig. S2b), which agreed with the observed crystal structure in the XRD.

The chemical and valence states of NiCo LDH and Ru-NiCo LDH were examined by X-ray photoelectron spectroscopy (XPS). The XPS survey spectra (Fig. S3) shows the peaks of Ni, Co, Ru, O, and C at their respective binding energies, indicating the purity of the materials. The Ru 3d

peaks were deconvolved by fitting the data with Ru $3d_{5/2}$ and Ru $3d_{3/2}$ at 279.8 eV and 284.3 eV, respectively (Fig. S4), which reflects the presence of Ru^0 [25]. For the Ru-NiCo LDH, the spin orbit doublet peaks of Ni 2p are located at 856.2 and 874.0 eV while that of Co 2p centered at 780.4 and 795.5 eV with each showing two shakeup satellites in the deconvoluted XPS spectra (Figs. S5 and S6), indicating a variable oxidation state of +2 and + 3 [26,27]. Compared to the NiCo LDH, the Ni and Co XPS of Ru-NiCo LDH positively shifted by 0.2 and 0.3 eV, which suggests a higher valence state of Ni and Co or surface local electron density perturbation after Ru incorporation [28,29]. Previous reports have shown that high-valence Ni/Co not only favors the active phase formation of metal oxyhydroxides, but also optimizes the oxyhydroxide electronic structure to facilitate water oxidation kinetics [30]. The core-level of O 1s spectra can be deconvoluted into three spin–orbit peaks (Fig. S7). The O 1s peak signals located at 529.3, 531.4, and 532.6 eV can be respectively assigned to oxygen bonded to metal (M–O), low coordinated oxygen, and adsorbed hydroxy, or H_2O [31]. The O 1s in NiCo LDH positively shifted to higher binding energy compared to the O 1s XPS of Ru-NiCo LDH, indicating intimate coordination between Ru single atoms and O atoms in the NiCo LDH support. The valence and electronic local coordination of Ru-NiCo LDH and NiCo LDH were investigated using X-ray absorption near-edge structure (XANES) spectroscopy and extended X-ray absorption fine structure (EXAFS) spectroscopy. The Ru K-edge XANES spectra lies between those of Ru Foil and RuO_2 (Fig. 2a), indicating a positively charged metal environment. In the Fourier Transformed EXAFS (FT-EXAFS) spectra (Fig. 2b), the

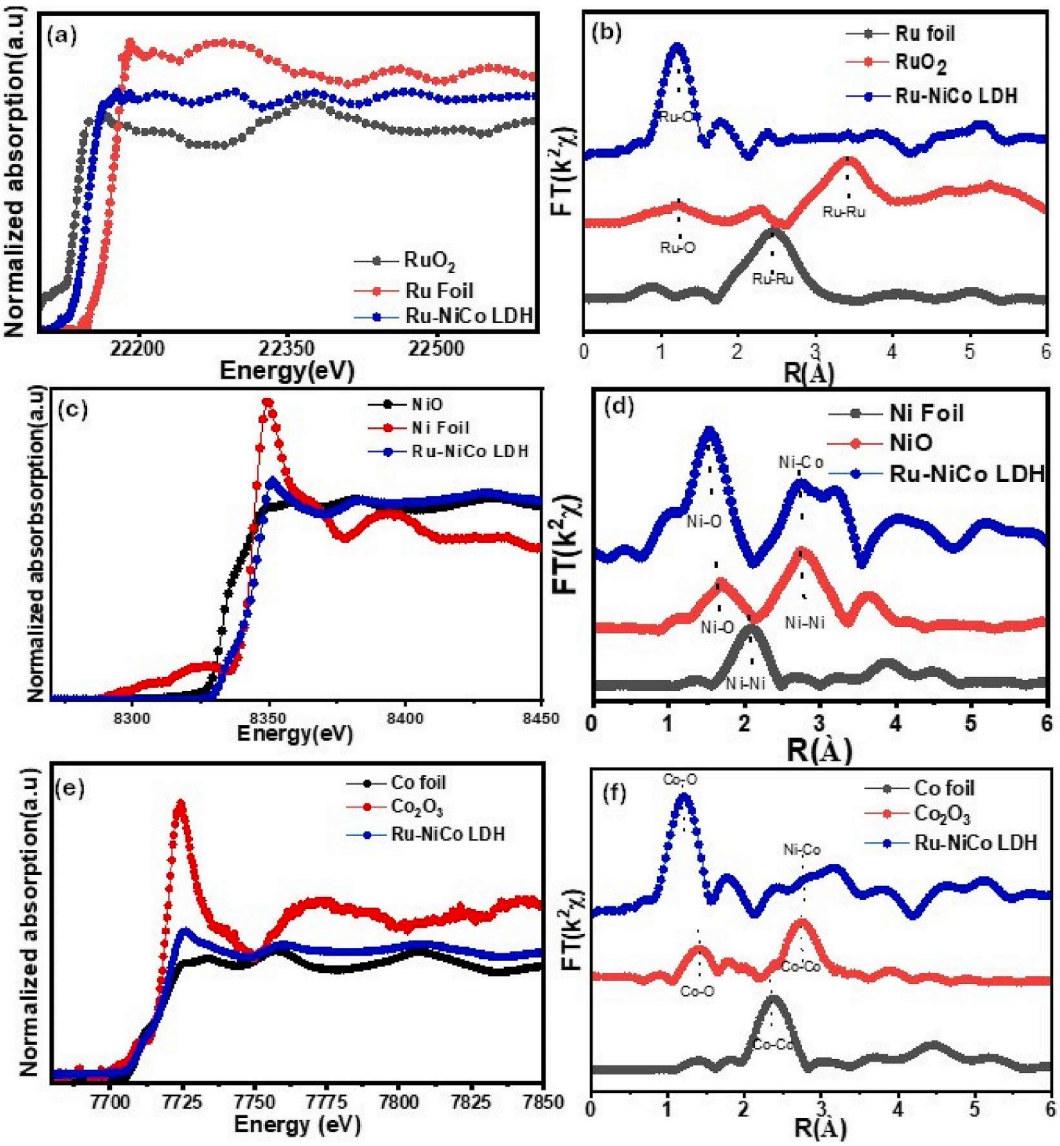

Fig. 2. X-ray absorption spectroscopy characterizations. (a, c, e) XANES spectra at Ru, Ni and Co K-edge of R-NiCo LDH along with reference standards, (b, d, f) corresponding Fourier-transform EXAFS spectra from a, d, and e.

strong Ru-O peak of the first shell was observed at an R-space of 1.28 Å and very weak Ru-O-M (M = Ni or Co) in the higher shells. The absence of characteristic peaks of Ru-Ru scattering in the R-NiCo LDH compared to Ru foil and RuO_2 indicates that the Ru is atomically dispersed on the NiCo LDH nanosheet [20,32], which is consistent with the analysis of the aberration-corrected TEM image.

For the investigation of the effect of the atomically dispersed Ru atoms on the NiCo LDH nanosheet, the XAFS analysis of the Ni and Co K edge and corresponding FT-EXAFS were performed (Fig. 2c–f). The Ni K-edge spectra of Ru-NiCo LDH and NiO showed a similar pre-edge peak around 8332.7 eV (Fig. 2c), suggesting that Ni could be in a +2-oxidation state. The prominent coordination peaks located at R-space of 1.48 and 2.72 Å (Fig. 2d) (phase uncorrected distance) can be assigned to Ni-O and Ni-Co/Ni. Similarly, the Co K-edge in the Ru-NiCo LDH observed at R-space of 7115.3 eV is identical to that of Co_2O_6, indicating the existence of Co with an oxidation state of +3. A distorted octahedral coordination geometry of the Co^{3+} sites in Ru-NiCo LDH is probably indicated by a slightly higher pre-edge intensity of Co_2O_3 (Fig. 2e). A strong Co-O peak of the first shell was observed at R-space of 1.35 Å while Co-O-M coordination weakens at higher shell (Fig. 2f). Comparing the Ni and Co K-edge XANES spectra of the Ru-NiCo LDH and NiCo LDH (Fig. S8), the absorption edge of Ni and Co in Ru-NiCo LDH show a positive shift relative to that in NiCo LDH, suggesting a higher valence state of Ni and Co [33], which agrees with the XPS results. Additionally, the EXAFS of Ru-NiCo LDH display two prominent peaks located around 1.58 and 2.83 Å (Fig. S8 c), which correspond to the nearest-neighbor Ni-O and Ni-Ni/Co coordination [34]. The Co R-space EXAFS spectra do not show any significant change for Co-O in Ru-NiCo LDH and NiCo LDH. Based on the above observations, the X-ray absorption spectroscopy analysis indicates that the introduced Ru is in the form of a single atom can increase the oxidation state of both Ni and Co elements, which is favorable for enhancing intrinsic activity toward water oxidation [35].

3. Electrochemical performance

The Ru-NiCo LDH catalyst was evaluated for electrochemical HER and OER performance using N_2-saturated 0.5M aq. H_2SO_4 and 1 M KOH as electrolytes. The different Ru loading was tested for HER to obtain the optimal amount required. Ru-NiCo LDH with 0.3 wt% loading requires an overpotential of 150 mV vs. RHE to deliver 10 mA (Fig. S9) while 0.52 wt% loading showed enhanced HER and requires only 20 mV vs.

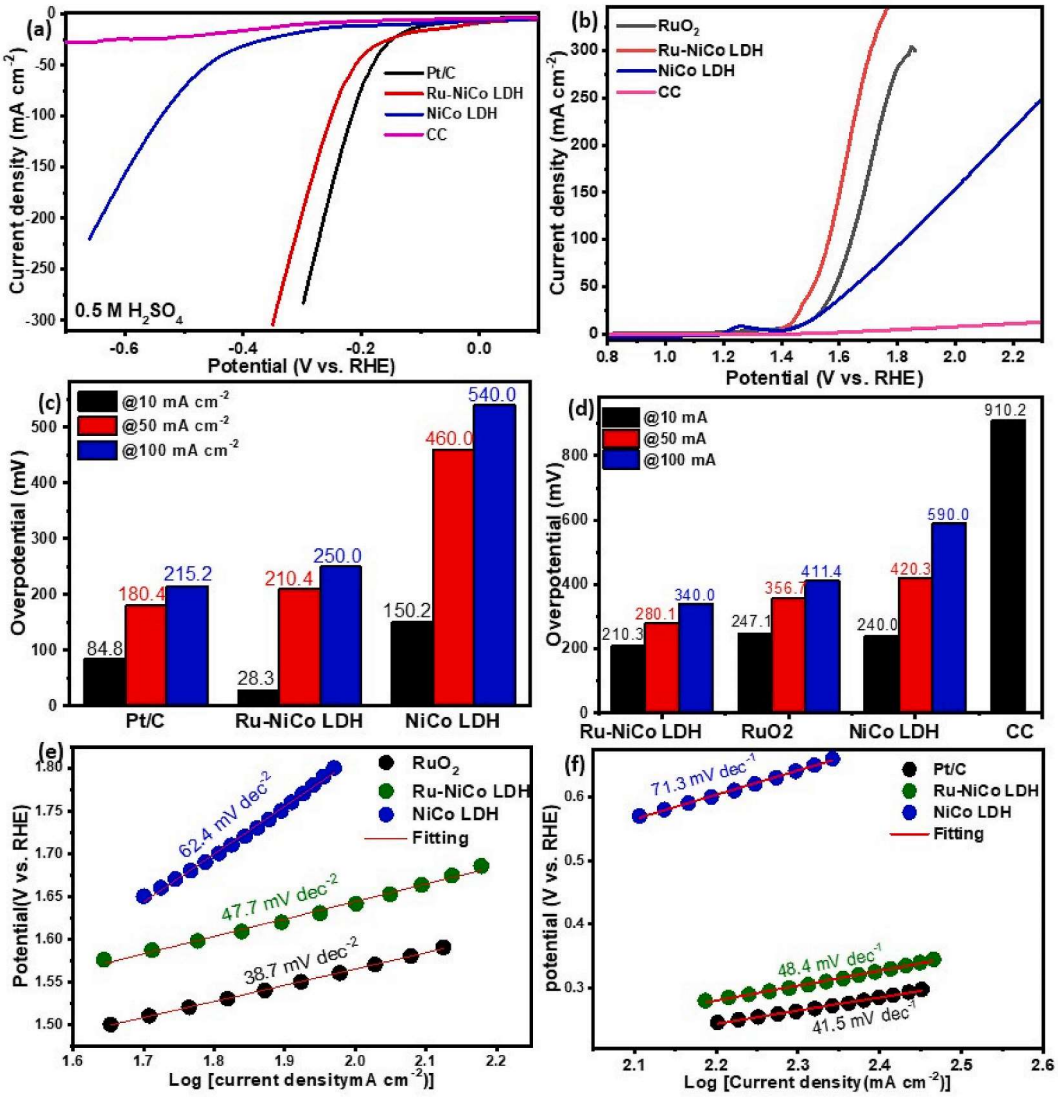

Fig. 3. Electrocatalytic HER and OER performance of Ru-NiCo LDH compared with NiCo LDH and commercial reference catalyst (Pt/C and RuO_2). (a, b) HER and OER polarization curves obtained at a scan rate of 5 mV s^{-1} in N_2-saturated 0.5 M H_2SO_4 (c, d) comparison of overpotential to achieve 10, 50 and 100 mA cm^{-2} for HER and OER (e, f) Tafel plots of catalysts.

RHE to deliver 10 mA current. A further increase in loading of 1.12 wt% results in reduced performance. A long-standing scientific challenge, especially for industrial applications, is the high loading of non-noble metal catalysts without losing active sites [36,37]. High loading affects both electron transport in the electrode active material and ion transport in the electrolyte, resulting in a deviation of apparent catalytic activity from actual intrinsic catalytic performance [37]. It is anticipated that higher Ru loading results in the blockage of the ion penetration and electron transport pathways. Thus, only Ru-NiCo LDH with 0.52 wt% loading was used for further studies. The commercial Pt/C and RuO_2 as well as bare carbon cloth (CC) were tested as reference along with the Ru-NiCo LDH and NiCo LDH under the same conditions. As shown in Fig. 3a and b, the CC did not display any catalytic activity for HER or OER within the applied potential window. Contrarily, both Pt/C, RuO_2, Ru-NiCo LDH, and NiCo LDH show excellent activity toward the HER and OER reactions under acidic conditions (Fig. 3a and b). For HER, the Ru-NiCo LDH shows superior electrocatalytic activity with small overpotentials of 28.3, 210.4, and 250 mV at 10, 50, and 100 mA cm^{-2} (Fig. 3c), respectively, compared to NiCo LDH (overpotentials of 150.2, 460, and 540 mA cm^{-2}) and Pt/C (84.8, 28.3 and 150.2 mV at 10, 50 and 100 mA cm^{-2}). As factor that influences effective water splitting, it has been shown that the influence of mass transfer dominates at high current densities while the Tafel slope is the main indicator at the low current densities [38]. In acidic medium, it is probable that Ru-NiCo LDH exhibits faster charge/electron transfer at low current density due to strong dissociative hydrogen adsorption to the Co-site [39]. As the current density increases, the mass transfer in the Pt/C increases and surpasses that of Ru-NiCo, which results in lower overpotential for the former than the later. The Ru-NiCo LDH also exhibits a smaller Tafel slope of 47.7 mA dec^{-2}, which is very close to that of Pt/C, indicating that the rate determining step is the chemisorption of hydrogen, following the Volmer-Tafel mechanism [40,41]. Similarly, the OER maintains the same trend, with Ru-NiCo LDH showing superior performance than NiCo LDH and benchmark RuO_2 (Fig. 3e–f).

In alkaline media, the HER and OER of the catalysts were evaluated in a solution of N_2-saturated 1.0 M aq. KOH (Fig. 4). Compared with NiCo LDH, the HER for Ru-NiCo LDH catalyst requires a smaller overpotential of 142.8, 231.3, and 267.8 mV to deliver 10, 50, and 100 mA cm^{-2} current (Fig. 4a–c) and maintain a smaller Tafel slope of 39.7 mV dec^{-1}, which is close to that of Pt/C (31.3 mV dec^{-1}) (Fig. 4e),

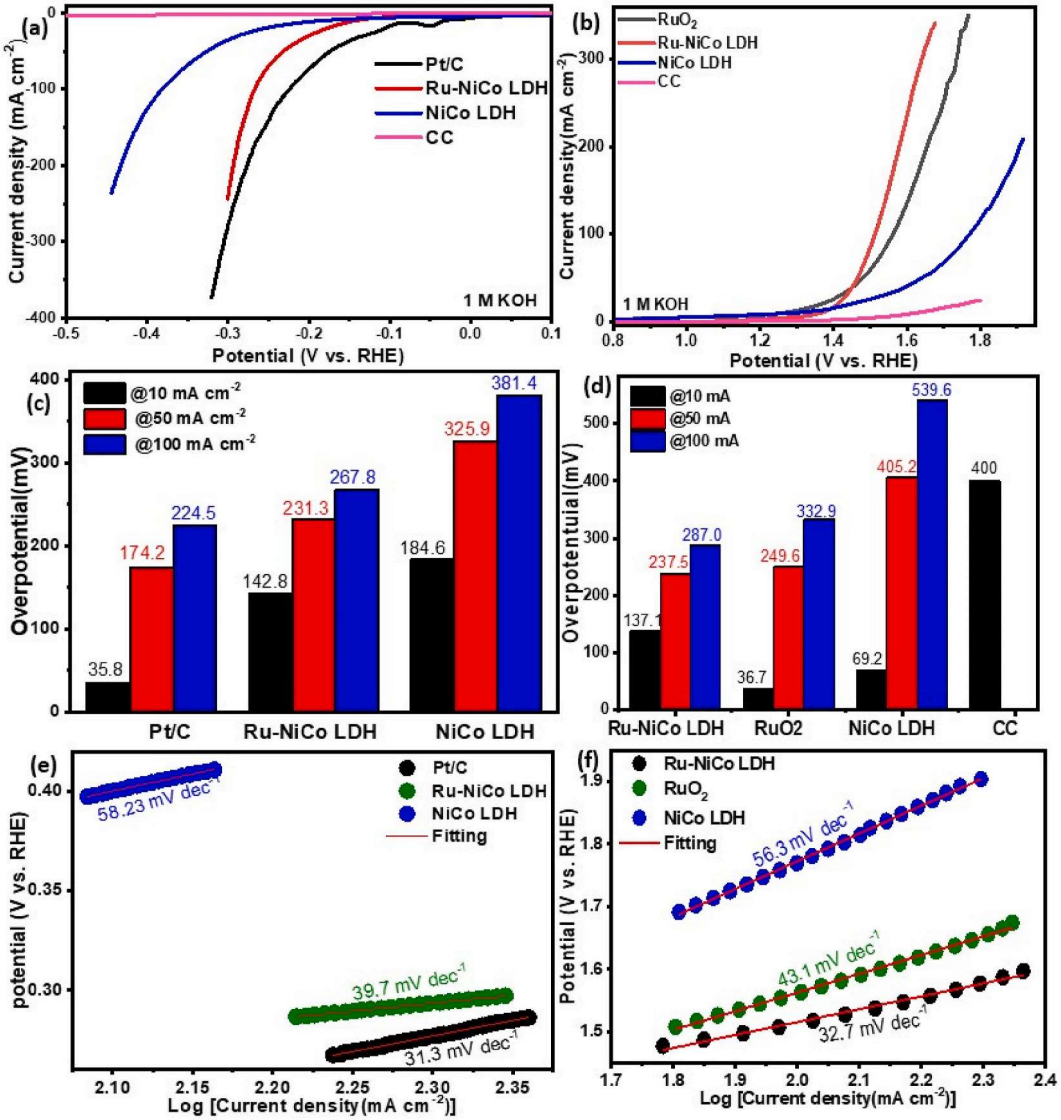

Fig. 4. Electrocatalytic HER and OER performance of Ru-NiCo LDH compared with NiCo LDH and commercial reference catalysts (Pt/C and RuO_2). (a, b) HER and OER polarization curves obtained at a scan rate of 5 mV s^{-1} in N_2-saturated 1 M KOH, (c, d) comparison of overpotential to achieve 10, 50, and 100 mA cm^{-2} for HER and OER (e, f) Tafel plots of catalysts.

suggesting the ability for fast catalyzing of reaction. Similarly, for OER, the overpotential of Ru-NiCo LDH exhibits superior catalytic behaviors than benchmark RuO_2 (Fig. 4b–d). The OER catalytic kinetics was probed by the Tafel plots (Fig. 4f), in which Ru-NiCo LDH shows a smaller Tafel slope (32.7 mV dec^{-1}) than RuO_2 (43.1 mV dec^{-1}) and NiCo LDH (56.3 mV dec^{-1}) catalysts. The electrochemical active surface area (ECSA) which is directly related to double layer electrochemical capacitance (Cdl), was determined by measuring the near non-faradaic capacitive current associated with double layer charging using cyclic voltammetry at different scan-rate. Plotting the capacitive current against the scan rate (Fig. S11) gives a straight line with the average slope of the anodic and cathodic current equal to Cdl. From the linear slope of the Cdl values, the electrochemical active surface area (ECSA) was estimated. The ECSA for Ru-NiCo LDH electrodes (21.33 m^2 g^{-1}) is much larger than that of NiCo LDH (9.58 m^2 g^{-1}), which indicates greater electroactive area in the former compared to the latter. The superior catalytic performance of the Ru-NiCo LDH for water splitting could be attributed to the Ru single atom tailoring effect. The Ru single atom species could electronically modify the surrounding Ni-Co atoms, reducing their hydrogen binding energy to the near-optimal HER activity region and giving NiCo species greater stability against overoxidation under OER conditions.

4. Theoretical study

To identify the active site in the Ru-NiCo LDH, first principle DFT calculations were performed, and the Gibbs free energy for each elementary reaction step in HER and OER were investigated. A prerequisite key descriptor for evaluating HER performance is the hydrogen absorption energy (ΔGH*) [20,42]. The Ru-NiCo LDH exhibits a lower (ΔGH*) of 0.19 eV compared with that of NiCo LDH (ΔGH* of 0.43 eV), indicating a more favorable enthalpy of hydrogen adsorption for Ru-NiCo LDH and a simultaneous decrease in the thermodynamic barriers for hydrogen production. The HER in the Co site features lower (ΔGH*) compared to the Ni and Ru sites (Fig. S13 a, b), suggesting that Co is the active site of HER in the Ru-NiCo LDH. The relative electronegativity difference between Ni (1.91) and Co (1.88) as well as the variable oxidation state of Co can regulate surface adsorption resulting in modified electronic structure and d-band centers. This agreed well with the recent report of Liu et al. in NiCo LDH [43].

The DFT modeling of the water oxidation mechanism, which involves four concerted proton-electron transfer steps, has also been

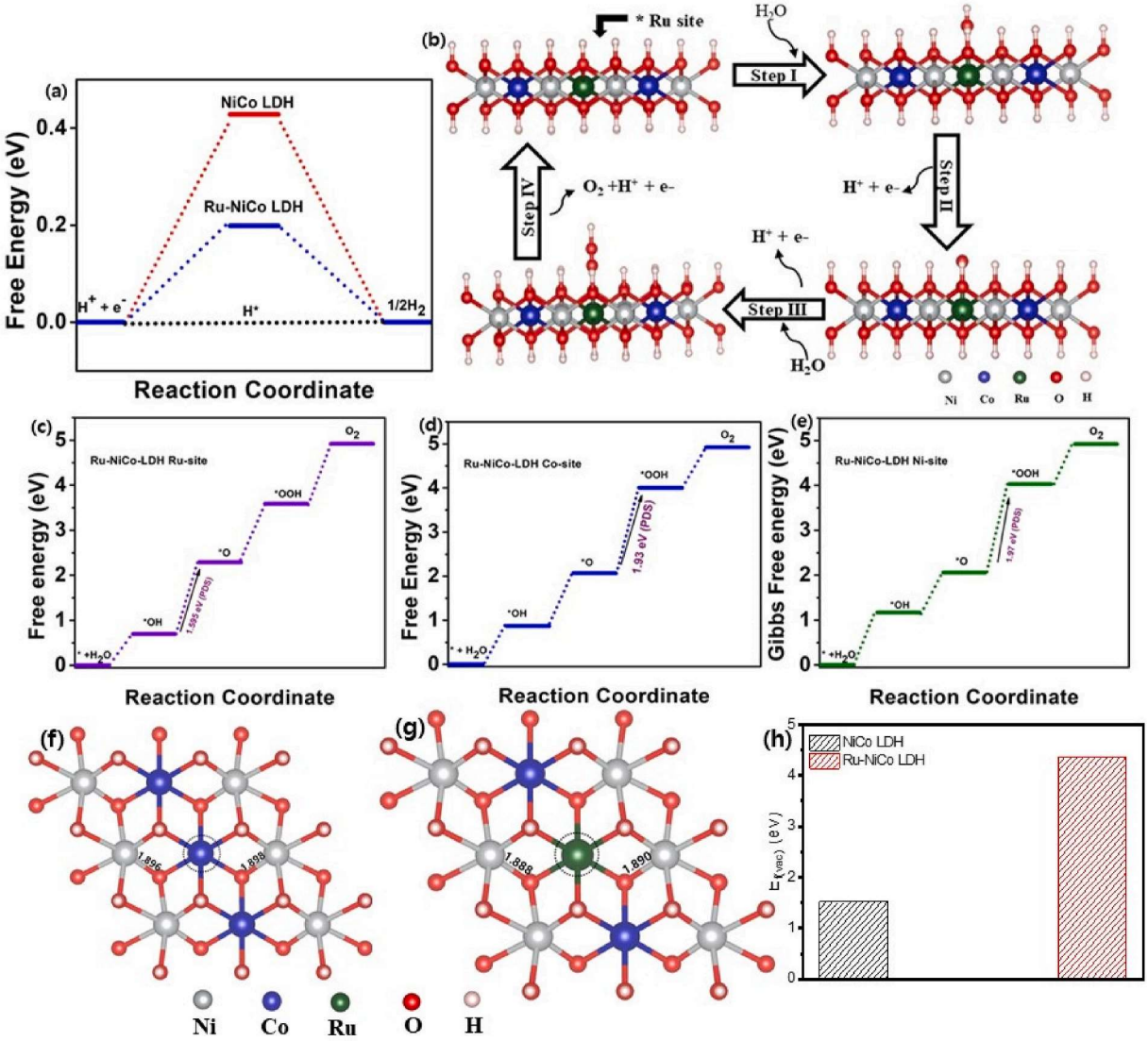

Fig. 5. DFT calculations. (a) HER free energy change for Ru-NiCo LDH and NiCo LDH, (b) Schematic illustration of the proposed OER mechanism and (c–e) Gibbs free energy diagram for a Ru, Co and Ni sites on Ru-NiCo LDH. The solid arrow with the number label in (c–e) indicates the rate-determining step. (f, g) Crystal plane structures of NiCo LDH and Ru-NiCo LDH with labeled Ni-O bond lengths (Å). (h) Ni vacancy formation energy ($E_{f(vac)}$) of NiCo LDH and Ru-NiCo LDH.

analyzed, and the Gibbs free energy for each elementary reaction is shown in Fig. 6c–e. For NiCo LDH, the rate determining step for the Co site and Ni site is the transition from O* to OOH* and the formation of O* from OH* respectively (Fig. S13 c, d). The rate determining steps in Co and Ni sites in NiCo LDH exhibit large Gibbs free energies, which lead to low O_2 rates; hence present sluggish OER kinetics.

The DFT results show that the rate-determining step for the Ru site on Ru-NiCo LDH is the transition HO* to O*, with an overpotential of 0.365 eV (Fig. 6b and c), which is lower than those of Co–O and Ni–O sites, hence expediting the OER kinetics. Interestingly, the Gibbs free energy of Ru sites is lower than those of Co and Ni sites both in NiCo LDH and Ru-NiCo LDH, which suggests that Ru is the active site for electrocatalytic OER performance. The Ru 3d peak in the DOS of Ru-NiCo LDH shows significant enhancement near the Fermi level (Fig. S13 e), which endows it with superior conductivity and charge transfer ability. Similarly, the PDOS of Ru-NiCo LDH also shows an enhanced peak close to the fermi energy level compared to NiCo LDH (Fig. S13 f), confirming the superior performance. To investigate the stability strength and role of the Ni site for Ru-NiCo LDH, the bond length in Ni-O and the formation energy arising from Ni vacancies (E_{vac}) were calculated by DFT

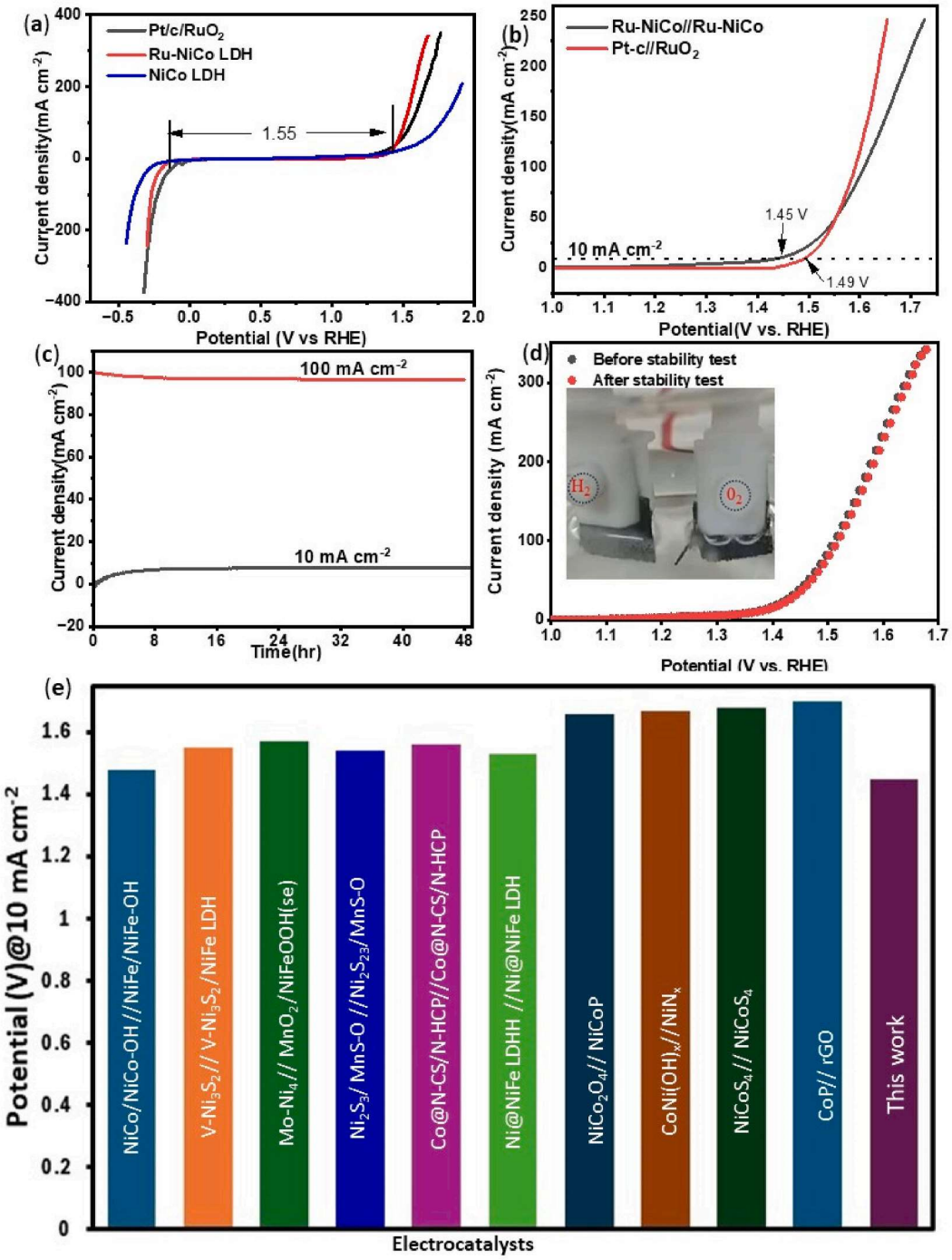

Fig. 6. Electrochemical overall water splitting (a) The overall polarization curves of catalysts within OER and HER potential window. (b) The polarization curve of Ru-NiCo//Ru-NiCo and Pt/C//RuO_2 in 1 M KOH with a scan rate of 5 mV s^{-1} for overall water-splitting in a two-electrode configuration. (c) The stability curve of the Ru-NiCo//Ru-NiCo at 10 and 100 mA cm^{-2} in 1 M KOH. (d) LSV polarization profile of the Ru-NiCo//Ru-NiCo before and after 48 h stability test. (e) Comparison of the cell voltages at the current density of 10 mA cm^{-2} for overall water splitting in this work with other reported bifunctional electrocatalysts.

(Fig. 5f). A shorter bond length was observed for the Ni-O in Ru-NiCo LDH compared to NiCo LDH, indicating a stronger Ni-O bond strength in the former, which is vital in creating a stable existence of Ni elements in the Ru-NiCo LDH lattice [44]. Additionally, the calculated Ni vacancy energy of formation (E_{vac}) in Ru-NiCo LDH is 3.36 eV (Fig. 5h), which is much higher than that of NiCo LDH (1.52 eV), also indicating that the Ru single atom incorporation into NiCo LDH could inhibit the Ni-O bond breaking and enhance the dissolution of Ni elements in the electrolyte, thereby strengthening the structure stability of Ru-NiCo [45]. To experimentally validate the theoretical calculation results, inductively coupled plasma optical emission spectrometry (ICP-OES) was used to measure the concentration of metallic ions in the electrolyte after long-term stability test for OER, and the result is presented in Table S1. The test showed that the concentration of Ni ions in the electrolyte after the stability test of Ru-NiCo LDH (0.024 mg L^{-1}) was significantly lower than that after the stability test of NiCo LDH (0.6126 mg L^{-1}), confirming the theoretical result. Thus, both the theoretical calculation and experimental results validate the fact that single atom Ru-induced Ni-O bond strength enhances the long-term durability.

5. Electrocatalytic activity of Ru-NiCo LDH toward overall water splitting

The excellent catalytic performance of Ru-NiCo LDH toward HER and OER inspired us to investigate the overall water splitting properties of the electrode material. A home-made two electrode configuration was used, with Ru-NiCo LDH serving simultaneously as both anode and cathode for water oxidation and reduction in 1.0 M KOH and 0.5 M H_2SO_4 respectively. The overall water splitting polarization curves for reversible HER and OER are shown in Fig. 6a. The change in potential between OER and HER ($\Delta V = E_{OER} - E_{HER}$) for Ru-NiCo LDH at 10 mA cm^{-2} is about 1.55 V, lower than the 1.62 V observed for NiCo LDH. The overall water splitting performance in alkaline media (Fig. 6b) reveals that Ru-NiCo/Ru-NiCo LDH pair required a low voltage of 1.45 V to drive the current density to 10 mA cm^{-2}, which is even lower than 1.49 V for the state-of-the-art Pt/C//RuO_2. The energy efficiency arising from the Ru-NiCo || Ru-NiCo couple cell can be calculated using equation (1):

$$\eta_{electrolyser} = \frac{E_{th}}{V_i} \times 100 \quad (1)$$

where $E_{th} = 1.23$ V and V_i (1.55 V) is the input cell voltage at 10 mA cm^{-2}. The calculated energy efficiency using the above equation is 79.35 %, which is comparable to the values reported in literature [46,47].

. In acidic media, the Ru-NiCo || Ru-NiCo couple required a cell voltage of 1.49 V to reach the current density of 10 mA cm^{-2}, also lower than the Pt/C//RuO_2 pair (Fig. S14). The slight enhanced performance in alkaline media compared to acidic media can be attributed to degradation of catalyst/electrode arising from acid corrosion [48].

Additionally, the symmetric two-electrode stability profile at 10 and 100 mA cm^{-2} revealed that the current density of the Ru-NiCo//Ru-NiCo couple can respectively maintain 96.7 % and 92.3 % of its initial value at a driving cell voltage of 1.55 V during the 48 h stability test (Fig. 6c), which indicates highly efficient and stable performance of the Ru-NiCo//Ru-NiCo composite as the bifunctional-electrocatalyst for overall water splitting. The Ru-NiCo//Ru-NiCo show lower stability in acidic media with 89.92 % remaining after 48 h testing period (Fig. S15), which can be attributed to the electrode corrosion. The negligible difference in LSV curve before and after the long-term durability test (Fig. 6d) of the Ru-NiCo/Ru-NiCo electrocatalyst further confirms the robust stability and long-term operational efficiency of the material. At applied potential of 1.55 V, vigorously formed hydrogen and oxygen bubbles could be visibly seen on the anode and cathode (Fig. 6d, insert, Movie S1). The comparative analysis of the Ru-NiCo// Ru-NiCo bifunctional catalysts with diverse non-noble metal bifunctional catalysts [49–58] at a current density of 10 mA cm^{-2} indicates superior catalytic performance for the Ru-NiCo//Ru-NiCo electrode pair, hence possesses great potential for application in overall water splitting.

Supplementary video related to this article can be found at https://doi.org/10.1016/j.renene.2024.121307.

6. Conclusion

In summary, a simple and scalable synthetic approach for atomic dispersion of large number of Ru single atoms on porous NiCo LDH is described. The Ru-NiCo LDH exhibits superior HER and OER in both acidic and alkaline media with low overpotential, high current density, and long-term durability due to the precise regulation of local coordination environments. The well-defined structures of the catalysts also make it possible to study the fundamental steps of the reaction in detail and to investigate the kinetics of the HER and OER reactions. DFT calculations show that Ru-NiCo LDH improves the favorable H adsorption energies toward HER and facilitates the coupling of O–O for OER. Ru-NiCo LDH//Ru-NiCo LDH provides an ultra-low overpotential of 1.45 mV at 10 mA cm^{-2} for the overall water splitting, which surpasses that of the state-of-the-art Pt/C/RuO_2 redox couple.

7. Experimental

7.1. Preparation of NiCo LDH and Ru-NiCo LDH

The synthesis of NiCo LDH (mass loading 9.62 mg cm^{2}) was accomplished following reported method [59]. A three-electrode cell configuration was used for the electrodeposition using NiCo LDH on carbon cloth as the working electrode, a graphite rod as the counter electrode, and a saturated Ag/AgCl (3 M) as the reference electrode. The electrodeposition of atomically dispersed Ru was carried via cycling NiCo LDH/CC (1 cm^{-2}) substrate from −0.5 to 0.5 V vs. Ag/AgCl at the sweep rate of 10 mV s^{-1} in the electrolyte (15 mL) containing $RuCl_3$ (1 mmol L^{-1}) and H_2SO_4 (0.1 mol L^{-1}) for 30 cycles at 25 °C. The Ru-NiCo LDH was removed after deposition and rinsed with deionized water several times and dried by nitrogen flow. The concentration of Ru in the electrolyte before and after deposition was quantitatively measured using inductively coupled plasma mass spectrometry to ascertain the loading for Ru on NiCo/CC. Detailed characterization, electrode fabrication and DFT calculations can be found in supporting information.

Data availability

The data that support the findings of this work are available from the corresponding author upon reasonable request.

CRediT authorship contribution statement

Njemuwa Nwaji: Writing – original draft, Methodology, Investigation, Funding acquisition, Formal analysis, Conceptualization. **Boka Fikadu:** Validation, Software, Data curation. **Magdalena Osial:** Writing – review & editing, Validation, Investigation, Data curation. **Birhanu Bayissa Gicha:** Writing – review & editing, Methodology, Investigation, Formal analysis. **Magdalena Warczak:** Writing – review & editing, Validation, Investigation, Formal analysis. **Hao Fan:** Writing – review & editing, Investigation, Data curation. **Jaebeom Lee:** Writing – review & editing, Investigation, Funding acquisition, Data curation. **Michael Giersig:** Writing – review & editing, Methodology, Investigation, Data curation.

Declaration of competing interest

The authors declare the following financial interests/personal relationships which may be considered as potential competing interests:

Jaebeom Lee reports financial support was provided by National

Research Foundation of South Korea. If there are other authors, they declare that they have no known competing financial interests or personal relationships that could have appeared to influence the work reported in this paper.

Acknowledgements

B. K, B. B. G and JL would like to acknowledge the National Research Foundation of Korea through grant (No. 2021K1A3A1A16096990, 2019K1A3A1A18116066. and Ministry of Trade, Industry and Energy of Korea (No. 20025720), M. Warczak would like to thank the National Science Center (NCN, Poland) for financial support through grant SONATA No. 2022/47/D/ST4/01421.

Appendix A. Supplementary data

Supplementary data to this article can be found online at https://doi.org/10.1016/j.renene.2024.121307.

References

[1] J. Das, H. Hu, P.P. Sahu, Nickel-nitride composite: water splitting with screw pitched cylindrical electrode and Fe(OH)2 catalyst under 1.4 V, Renew. Energy 165 (2021) 525.
[2] M.Z. Abid, K. Rafiq, A. Rauf, R.H. Althomali, R. Jin, E. Hussain, Interface engineering of $BiVO_4/Zn_3V_2O_8$ heterocatalysts for escalating the synergism: impact of Cu electron mediator for overall water splitting, Renew. Energy 225 (2024) 120223.
[3] S. Vinoth, A. Pandikumar, Ni integrated S-gC_3N_4/BiOBr based Type-II heterojunction as a durable catalyst for photoelectrochemical water splitting, Renew. Energy 173 (2021) 507.
[4] M. Duraivel, S. Nagappan, K. Prabakar, Anion intercalated nickel iron hydrogen phosphate hydrate for full water splitting application, Renew. Energy 219 (2023) 119529.
[5] J. Wang, Z. Guo, M. Liu, Y. Wang, H. Liu, L. Wu, Y. Xue, N. Cai, H. Li, $CoMoO_4$ nanoparticles decorated ultrathin nanoplates constructed porous flower as an electrocatalyst toward overall water splitting and Zn-air batteries, Renew. Energy 212 (2024) 751.
[6] K. Jiang, B. Liu, M. Luo, S. Ning, M. Peng, Y. Zhao, Y.-R. Lu, T.-S. Chan, F.M.F. de Groot, Y. Tan, Single platinum atoms embedded in nanoporous cobalt selenide as electrocatalyst for accelerating hydrogen evolution reaction, Nat. Commun. 10 (2019) 1743.
[7] S. Yan, W. Liao, M. Zhong, W. Li, C. Wang, N. Pinna, W. Chen, X. Lu, Partially oxidized ruthenium aerogel as highly active bifunctional electrocatalyst for overall water splitting in both alkaline and acidic media, Appl. Catal. B Environ. 307 (2022) 121199.
[8] K. Jiang, M. Luo, M. Peng, Y. Yu, Y.-R. Lu, T.-S. Chan, P. Liu, F.M.F. de Groot, Y. Tan, Dynamic active-site generation of atomic iridium stabilized on nanoporous metal phosphides for water oxidation, Nat. Commun. 11 (2020) 2701.
[9] X. Cai, Z. Zeng, Y. Liu, Z. Li, X. Gu, Y. Zhao, L. Mao, J. Zhang, Visible-light-driven water splitting by yolk-shelled ZnIn2S4-based heterostructure without noble-metal co-catalyst and sacrificial agent, Appl. Catal. B Environ. 297 (2021) 120391.
[10] Z. Li, X. Zhang, Z. Zhang, P. Chen, Y. Zhang, X. Dong, Dual-metal hydroxide@oxide heterojunction catalyst constructed via corrosion engineering for large-current oxygen evolution reaction, Appl. Catal. B Environ. 325 (2023) 122311.
[11] J. Wang, Y. Gao, H. Kong, J. Kim, S. Choi, F. Ciucci, Y. Hao, S. Yang, Z. Shao, J. Lim, Non-precious-metal catalysts for alkaline water electrolysis: operando characterizations, theoretical calculations, and recent advances, Chem. Soc. Rev. 49 (2020) 9154–9196.
[12] X. He, X. Han, X. Zhou, J. Chen, J. Wang, Y. Chen, L. Yu, N. Zhang, J. Li, S. Wang, H. Jin, Electronic modulation with Pt-incorporated NiFe layered double hydroxide for ultrastable overall water splitting at 1000 mA cm−2, Appl. Catal. B Environ. 331 (2023) 122683.
[13] S. Zhou, J. Wang, J. Li, L. Fan, Z. Liu, J. Shi, W. Cai, Surface-growing organophosphorus layer on layered double hydroxides enables boosted and durable electrochemical freshwater/seawater oxidation, Appl. Catal. B Environ. 332 (2023) 122749.
[14] S.M.N. Jeghan, D. Kim, Y. Lee, M. Kim, G. Lee, Designing a smart heterojunction coupling of cobalt-iron layered double hydroxide on nickel selenide nanosheets for highly efficient overall water splitting kinetics, Appl. Catal. B Environ. 331 (2022) 121221.
[15] J. Hou, Y. Wu, B. Zhang, S. Cao, Z. Li, L. Sun, Rational design of nanoarray architectures for electrocatalytic water splitting, Adv. Funct. Mater. 29 (2019) 1808367.
[16] Y. Tang, Q. Liua, L. Dong, H.B. Wu, X.Y. Yu, Activating the hydrogen evolution and overall water splitting performance of NiFe LDH by cation doping and plasma reduction, Appl. Catal., B 266 (2020) 118627.
[17] D. Yan, Y. Li, J. Huo, R. Chen, L. Dai, S. Wang, Defect chemistry of nonprecious metal electrocatalysts for oxygen reactions, Adv. Mater. 29 (2017) 1606459.
[18] Z.W. Gao, J.Y. Liu, X.M. Chen, X.L. Zheng, J. Mao, H. Liu, T. Ma, L. Li, W.C. Wang, X.W. Du, Engineering NiO/NiFe LDH intersection to bypass scaling relationship for oxygen evolution reaction via dynamic tridimensional adsorption of intermediates, Adv. Mater. 31 (2019) 1804769.
[19] P. Li, M. Wang, X. Duan, L. Zheng, X. Cheng, Y. Zhang, Y. Kuang, Y. Li, Q. Ma, Z. Feng, W. Liu, X. Sun, Boosting oxygen evolution of single-atomic ruthenium through electronic coupling with cobalt–iron layered double hydroxides, Nat. Commun. 10 (2019) 1711.
[20] J. Zhang, J. Liu, L. Xi, Y. Yu, N. Chen, S. Sun, W. Wang, K.M. Lange, B. Zhang, Single-atom Au/NiFe layered double hydroxide electrocatalyst: probing the origin of activity for oxygen evolution reaction, J. Am. Chem. Soc. 140 (2018) 3876–3879.
[21] T. Lim, G.Y. Jung, J.H. Kim, S.O. Park, J. Park, Y.-T. Kim, S.J. Kang, H.Y. Jeong, S. K. Kwak, S.H. Joo, Atomically dispersed Pt-N_4 sites as efficient and selective electrocatalysts for the chlorine evolution reaction, Nat. Commun. 11 (2020) 412.
[22] D. Liu, S. Chen, H. Yan, C. Wang, C. Wu, Y.A. Haleem, S. Duan, J. Lu, B. Ge, P. M. Ajayan, Y. Luo, J. Jiang, L. Song, Atomically dispersed platinum supported on curved carbon supports for efficient electrocatalytic hydrogen evolution, Nat. Energy 4 (2019) 512–518.
[23] J.V. Rojasa, M. Toro-Gonzaleza, M.C. Molina-Higginsa, C.E. Castanoba, Facile radiolytic synthesis of ruthenium nanoparticles on graphene oxide and carbon nanotubes, Mater. Sci. Eng., B 205 (2016) 28.
[24] Y. Zhao, X. Zhang, X. Jia, G.I.N. Waterhouse, R. Shi, X. Zhang, F. Zhan, Y. Tao, L.-Z. Wu, C.-H. Tung, D. O'Hare, T. Zhang, Sub-3 nm ultrafine monolayer layered double hydroxide nanosheets for electrochemical water oxidation, Adv. Energy Mater. 8 (2018) 1703585.
[25] D.J. Morgan, Resolving ruthenium: XPS studies of common ruthenium materials, Surf. Interface Anal. 47 (2015) 1072.
[26] F.I. Dionigi, Z. Zhenhua, S. Ilya, M. Thomas, D. Siddharth, L.M. Bernal, K. Sebastian, Z. Ioannis, S. Hannes, F. Dingxin, B. Arno, D. Jakub, D.J. Ferreira, G. Manuel, T. Detre, Z. Jing, L. Wei-Xue, G. Jeffrey, C.B. Roldan, S. Peter, In-situ structure and catalytic mechanism of NiFe and CoFe layered double hydroxides during oxygen evolution, Nat. Commun. 11 (2020) 2522.
[27] N. Nwaji, J. Gwak, M. Goddati, H. Kang, A.H. Pasanaje, A. Sharan, N. Singh, J. Lee, Defect-engineered Fe_3C@$NiCo_2S_4$ nanospike derived from Metal−Organic frameworks as an advanced electrode material for hybrid supercapacitors, ACS Appl. Mater. Interfaces 15 (2023) 34779–34788.
[28] N. Nwaji, G.M. Zewdie, J. Gwak, J. Kang, L.T. Tufa, Y. Choi, M. Goddati, H. Shin, J. Lee, J. Dimeric, Ni-Co single-atom anchored on ultrathin N-doped 2D molybdenum carbide boosted performance in solid-state supercapacitor, J. Energy Storage 83 (2024) 110671.
[29] N. Nwaji, H. Kang, M. Goddati, L.T. Tufa, J. Gwak, A. Sharan, N. Singh, J. Lee, Sulfur vacancy induced Co_3S_4@$CoMo_2S_4$ nanocomposite as functional electrode for high performance supercapacitor, J. Mater. Chem. A 11 (2023) 3640, 365.
[30] J. Yin, J. Jin, M. Lu, B. Huang, H. Zhang, Y. Peng, P. Xi, C.H. Yan, Iridium single atoms coupling with oxygen vacancies boosts oxygen evolution reaction in acid media, J. Am. Chem. Soc. 142 (2020) 18378.
[31] M. Asnavandi, Y. Yin, Y. Li, C. Sun, C. Zhao, Promoting oxygen evolution reactions through introduction of oxygen vacancies to benchmark NiFe–OOH catalysts, ACS Energy Lett. 7 (2018) 1515–1520.
[32] L. Song, D. Tian, H. Jiang, D. Cao, S. Wei, D. Liu, P. Song, Y. Lin, L. Song, Achieving efficient alkaline hydrogen evolution reaction over a Ni_5P_4 catalyst incorporating single-atomic Ru sites, Adv. Mater. 32 (2020) 1906972.
[33] L. Han, H. Cheng, W. Liu, H. Li, P. Ou, R. Lin, H.T. Wang, C.W. Pao, A.R. Head, C. H. Wang, X. Tong, C.J. Sun, W.F. Pong, J. Luo, J.C. Zheng, H.L. Xin, A single-atom library for guided monometallic and concentration-complex multimetallic designs, Nat. Mater. 21 (2022) 681.
[34] Q. Wang, X. Huang, Z.L. Zhao, M. Wang, B. Xiang, J. Li, Z. Feng, H. Xu, M. Gu, Ultrahigh-loading of Ir single atoms on NiO matrix to dramatically enhance oxygen evolution reaction, J. Am. Chem. Soc. 142 (2020) 7425.
[35] K. Shah, R. Dai, M. Mateen, Z. Hassan, Z. Zhuang, C. Liu, M. Israr, W.C. Cheong, B. Hu, R. Tu, C. Zhang, X. Chen, Q. Peng, C. Chen, Y. Li, Cobalt single atom incorporated in ruthenium oxide sphere: a robust bifunctional electrocatalyst for HER and OER, Angew. Chem., Int. Ed. 61 (2022) e202114951.
[36] N. Wang, R. Mei, X. Lin, L. Chen, T. Yang, Q. Liu, Z. Chen, Cascade anchoring strategy for fabricating high-loading Pt single atoms as bifunctional catalysts for electrocatalytic hydrogen evolution and oxygen reduction reactions, ACS Appl. Mater. Interfaces 15 (2023) 29195–29203.
[37] N. Khodayar, A. Noori, M.S. Rahmanifar, M. Moloudi, N. Hassani, M. Neek-Amal, M.F. El-Kady, N.B. Mohamed, X. Xia, Y. Zhang, R.B. Kaner, M.F. Mousavi, An ultra-high mass-loading transition metal phosphide electrocatalyst for efficient water splitting and ultra-durable zinc–air batteries, Energy Environ. Sci. 17 (2024) 5200–5215.
[38] Y. Luo, L. Tang, U. Khan, Q. Yue, X. Zou, B. Liu, Morphology and surface chemistry engineering toward pH-universal catalysts for hydrogen evolution at high current density, Nat. Commun. 10 (2019) 269–277.
[39] A.N. Pour, Z. Keyvanloo, M. Izadyar, S.M. Modaresi, Dissociative hydrogen adsorption on the cubic cobalt surfaces: a DFT study, Int. J. Hydrogen Energy 40 (2015) 7064.
[40] M. Cabán-Acevedo, M.L. Stone, J.R. Schmidt, J.G. Thomas, Q. Ding, H.-C. Chang, M.-L. Tsai, J.-H. He, S. Jin, Efficient hydrogen evolution catalysis using ternary pyrite-type cobalt phosphosulphide, Nat. Mater. 14 (2015) 1245.
[41] M.R. Gao, J.X. Liang, Y.R. Zheng, Y.F. Xu, J. Jiang, Q. Gao, J. Li, S.-H. Yu, An efficient molybdenum disulfide/cobalt diselenide hybrid catalyst for electrochemical hydrogen generation, Nat. Commun. 6 (2015) 5982.

[42] K. Jiang, B. Liu, M. Luo, S. Ning, M. Peng, Y. Zhao, Y.-R. Lu, T.S. Chan, F.M.F. de Groot, Y. Tan, Single platinum atoms embedded in nanoporous cobalt selenide as electrocatalyst for accelerating hydrogen evolution reaction, Nat. Commun. 10 (2019) 1743.
[43] H. Liu, Y. Jiang, Y. Mao, Y. Jiang, W. Shen, M. Li, R. He, The role of various components in Ru-NiCo alloys in boosting the performance of overall water splitting, J. Colloid Interface Sci. 633 (2023) 189–198.
[44] W. He, L. Han, Q. Hao, X. Zheng, Y. Li, J. Zhang, C. Liu, H. Liu, H.L. Xin, Fluorine-anion-modulated electron structure of nickel sulfide nanosheet arrays for alkaline hydrogen evolution, ACS Energy Lett. 4 (2019) 2905.
[45] F. Dionigi, J. Zhu, Z. Zeng, T. Merzdorf, H. Sarodnik, M. Gliech, L. Pan, W.-X. Li, J. Greeley, P. Strasser, Intrinsic electrocatalytic activity for oxygen evolution of crystalline 3d-transition metal layered double hydroxides, Angew. Chem., Int. Ed. 60 (2021) 14446.
[46] Y. Jiao, Y. Zheng, M. Jaroniec, S.Z. Qiao, Design of electrocatalysts for oxygen- and hydrogen-involving energy conversion reactions, Chem. Soc. Rev. 44 (2015) 2060.
[47] A. Ursua, L.M. Gandia, P. Sanchis, Proc. Hydrogen production from water electrolysis: current status and future trends, IEEE 100 (2012) 410.
[48] J. Kibsgaard, I. Chorkendorff, Considerations for the scaling-up of water splitting catalysts, Nat. Energy 4 (2019) 430.
[49] C.-F. Li, L.-J. Xie, J.-W. Zhao, L.-F. Gu, J.-Q. Wu, G.-R. Li, Interfacial electronic modulation by Fe_2O_3/NiFe-LDHs heterostructures for efficient oxygen evolution at high current density, Appl. Catal. B Environ. 278 (2020) 119326.
[50] J. Zhou, L. Yu, Q. Zhu, C. Huang, Y. Yu, Defective and ultrathin NiFe LDH nanosheets decorated on V-doped Ni_3S_2 nanorod arrays: a 3D core–shell electrocatalyst for efficient water oxidation, J. Mater. Chem. A 7 (2019) 18118.
[51] S. Niu, W.-J. Jiang, Z. Wei, T.T.J. Ma, J.-S. Hu, L.-J. Wan, Se-doping activates FeOOH for cost-effective and efficient electrochemical water oxidation, J. Am. Chem. Soc. 141 (2019) 7005.
[52] Y. Zhang, J. Fu, H. Zhao, R. Jiang, F. Tian, R. Zhang, Tremella-like Ni_3S_2/MnS with ultrathin nanosheets and abundant oxygen vacancies directly used for high-speed overall water splitting, Appl. Catal. B Environ. 257 (2019) 117899.
[53] Z. Chen, Y. Ha, H. Jia, X. Yan, M. Chen, M. Liu, R. Wu, Oriented transformation of Co-LDH into 2D/3D ZIF-67 to achieve Co–N–C hybrids for efficient overall water splitting, Adv. Energy Mater. 9 (2019) 1803918.
[54] Z. Cai, X. Bu, P. Wang, W. Su, R. Wei, J.C. Ho, J. Yanga, X. Wang, Simple and cost-effective fabrication of 3D porous core–shell Ni nanochains@NiFe layered double hydroxide nanosheet bifunctional electrocatalysts for overall water splitting, J. Mater. Chem. A 7 (2019) 21722.
[55] W. Jin, J. Chen, H. Wu, N. Zang, Q. Li, W. Cai, Z. Wu, Interface engineering of oxygen-vacancy-rich NiCo2O4/NiCoP heterostructure as an efficient bifunctional electrocatalyst for overall water Splitting, Catal. Sci. Technol. 10 (2020) 5559–5565.
[56] B. You, Y. Sun, Hierarchically porous nickel sulfide multifunctional superstructures, Adv. Energy Mater. 6 (2016) 1502333.
[57] D. Liu, Q. Lu, Y. Luo, X. Sun, A.M. Asiri, $NiCo_2S_4$ nanowires array as an efficient bifunctional electrocatalyst for full water splitting with superior activity, Nanoscale 7 (2015) 15122–15126.
[58] L. Jiao, Y.X. Zhou, H.L. Jiang, Metal-organic framework-based CoP/reduced graphene oxide: high-performance bifunctional electrocatalyst for overall water splitting, Chem. Sci. 7 (2016) 1690–1695.
[59] H. Liang, F. Meng, M. Cabán-Acevedo, L. Li, A. Forticaux, L. Xiu, Z. Wang, S. Jin, Hydrothermal continuous flow synthesis and exfoliation of NiCo layered double hydroxide nanosheets for enhanced oxygen evolution catalysis, Nano Lett. 15 (2015) 1421–1427.